Atmos. Chem. Phys. Discuss., 14, 919–951, 2014
www.atmos-chem-phys-discuss.net/14/919/2014/
doi:10.5194/acpd-14-919-2014

Atmospheric Chemistry and Physics Discussions

An evaluation of O_3 dry deposition simulations in East Asia

R. J. Park[1], S. K. Hong[1], H.-A. Kwon[1], S. Kim[2], A. Guenther[3], J.-H. Woo[4], and C. P. Loughner[5]

[1]School of Earth and Environmental Sciences, Seoul National University, Seoul, Korea
[2]Department of Earth System Science, University of California, Irvine, CA, USA
[3]Pacific Northwest National Laboratory, Richland, WA, USA
[4]Department of Environmental Engineering, Konkuk University, Seoul, Korea
[5]CMNS-Earth System Science Interdisciplinary Center, University of Maryland, College Park, MD, USA

Received: 2 December 2013 – Accepted: 20 December 2013 – Published: 13 January 2014

Correspondence to: R. J. Park (rjpark@snu.ac.kr)

Published by Copernicus Publications on behalf of the European Geosciences Union.

Abstract

We used a 3-D regional atmospheric chemistry transport model (WRF-Chem) to examine processes that determine O_3 in East Asia; in particular, we focused on O_3 dry deposition, which is an uncertain research area due to insufficient observation and numerical studies in East Asia. Here, we compare two widely used dry deposition parameterization schemes, Wesely and M3DRY, which are used in the WRF-Chem and CMAQ models, respectively. The O_3 dry deposition velocities simulated using the two aforementioned schemes under identical meteorological conditions show considerable differences (a factor of 2) due to surface resistance parameterization discrepancies. The O_3 concentration differed by up to 10 ppbv for the monthly mean. The simulated and observed dry deposition velocities were compared, which showed that the Wesely scheme model is consistent with the observations and successfully reproduces the observed diurnal variation. We conduct several sensitivity simulations by changing the land use data, the surface resistance of the water and the model's spatial resolution to examine the factors that affect O_3 concentrations in East Asia. As shown, the model was considerably sensitive to the input parameters, which indicates a high uncertainty for such O_3 dry deposition simulations. Observations are necessary to constrain the dry deposition parameterization and input data to improve the East Asia air quality models.

1 Introduction

Ozone (O_3) is a harmful air pollutant in surface air and the primary chemical oxidation driver in the free troposphere, and O_3 tropospheric concentrations are largely determined by the balance between net chemical production, influx from the stratosphere and physical-loss processes (Wu et al., 2007). O_3 dry deposition is a dominant physical loss process and accounts for approximately 25 % of the total O_3 lost in the troposphere (Lelieveld and Dentener, 2000).

ACPD
14, 919–951, 2014

In typical chemical transport models, dry deposition is calculated as a first-order process that uses dry deposition velocity, which is parameterized as a function of surface type and atmospheric stability conditions (Wesely, 1989). However, in models, its parameterization is highly uncertain due to complexities from surface conditions at sub-grid scales (Wu et al., 2011). Thus, previous studies on dry deposition calculations have primarily focused on the United States and Europe, for which observations on ozone fluxes or dry deposition velocities were available to validate either simulated O_3 losses or dry deposition velocity parameterization (Charusombat et al., 2010; Gerosa et al., 2007; Rannik et al., 2012; Wu et al., 2011).

East Asia (China, Japan, and Korea) has recently experienced rapid economic growth, during which anthropogenic emissions have increased and deteriorated air quality (Ohara et al., 2007). Thus, air quality model use has also gradually increased in East Asia to understand the air pollutant spatial and temporal distributions and examine the impact of the increased anthropogenic emissions on air quality degradation for East Asian countries. A critical role for such models includes quantifying the regional air quality sources, including trans-boundary transport of air pollutants and their precursors in East Asia. In this context, the dry deposition simulation is important for accurately assessing the contribution from a source to regional air pollutant concentrations.

However, air quality model evaluations have been relatively limited due to the lack of long-term regional observations in East Asia. In particular, evaluating individual processes, including dry deposition calculations, has not been rigorous for East Asia. Several O_3 dry deposition simulation studies have been conducted for a tropical forest in Southeast Asia (Matsuda et al., 2005, 2006), but the vegetation type differs from East Asia.

The purpose of this study is to evaluate the O_3 dry deposition simulations (schemes) in the most widely used regional air chemistry models in East Asia: the Weather Research and Forecasting-Chemistry (WRF-Chem) and the Community Multiscale Air Quality (CMAQ) models. We conducted multiple model simulations to understand the

ACPD
14, 919–951, 2014

differences between the two models as well as two different dry deposition schemes and factors that affect dry deposition and O_3 concentrations in East Asia. We also evaluated the O_3 concentration and dry deposition velocity model results by comparing such results with observations to constrain the model simulations. Finally, several sensitivity simulations were performed using different input datasets to demonstrate the models' uncertainty, which should be considered in assessing O_3 spatial and temporal distribution and contribution from a source to the a particular region, including trans-boundary transport of its precursors in East Asia.

2 Model description

2.1 General description

We used the WRF-Chem model (version 3.3) to simulate O_3 in East Asia. The model is a fully coupled meteorology-chemistry model, which was developed by the National Center for Atmospheric Research (NCAR) (Grell et al., 2005) to account for the interaction between meteorological and chemical processes at each time step (Chapman et al., 2009). The model is described in detail elsewhere (Grell et al., 2005). Herein, we primarily describe our model simulations.

The model has the horizontal resolutions 45 km × 45 km with 14 eta vertical grids and a 50 hPa top. The model domain for our simulations is shown in Fig. 1, which includes the nested grid domain that focuses on the Korean peninsula. For meteorology simulations, we used physics modules in the WRF, as shown in Table 1. In particular, turbulent mixing at the surface and within the planetary boundary layers was calculated using schemes developed by Chen and Dudhia (2001) and Hong et al. (2006), respectively.

We used anthropogenic emissions from the Sparse Matrix Operator Kernel Emissions-Asia (SMOKE-Asia), which was developed by Woo et al. (2011) to operate the CMAQ model (Byun and Ching, 1999) over East Asia. SMOKE-Asia calculates

ACPD
14, 919–951, 2014

anthropogenic emissions based on the Carbon Bond 05 (CB05) chemical mechanism (Appel et al., 2007), which slightly differs from the Carbon Bond mechanism Z (CBz) used in WRF-Chem. We used the chemical mapping in Table 2 to match the emission species between CB05 and CBz. A few species do not precisely correspond between the two schemes, but such species are relatively unimportant for our O_3 simulations below. The total NO_x, CO, and VOC emissions in the domain are 24.6 $Tg\,yr^{-1}$, 150.2 $Tg\,yr^{-1}$, and 96.0 $Tg\,yr^{-1}$, respectively.

The initial and lateral boundary conditions for the meteorology simulations were determined using a WRF preprocessing system with the NCEP Final Operational Model Global Tropospheric Analyses data (National Centers for Environmental Prediction, 2000). Climatological values were used to generate the initial and boundary values for the chemical species concentrations (Grell et al., 2005).

2.2 Dry deposition parameterization

Chemical species loss due to dry deposition in air chemistry models is typically computed as a first-order process, the dry deposition velocity for which is parameterized as shown in Eq. (1).

$$F = v_d C \tag{1}$$

v_d indicates the dry deposition velocity, and C represents the species concentrations in the lowest model layer. Therefore, the species lost to dry deposition is directly proportional to the dry deposition velocity, which is also parameterized in such models.

The dry deposition velocity is computed as the reciprocal of the sum for aerodynamic resistance (R_a), quasi-laminar resistance (R_b), and surface resistance (R_c) as follows:

$$v_d = \frac{1}{R_a + R_b + R_c}. \tag{2}$$

Therefore, in Eq. (2), the resistance with the largest value is the most important factor that determines dry deposition velocity. Generally, surface resistance is the largest

ACPD
14, 919–951, 2014

among the three resistances, and it determines the dry deposition velocity (Erisman et al., 1994); we will discuss the surface resistance formulation in Sect. 2.3.

Here, we compare two widely used dry deposition schemes: the Wesely and M3DRY schemes. The first scheme was developed by Wesely (1989) and is used in WRF-Chem as the default method (hereinafter, the Wesely method). The latter scheme was proposed by Pleim et al. (2001) and is used as a default scheme in CMAQ; it is a part of the meteorological transport module Meteorology-Chemistry Interface Processor version 3.3 used in CMAQ, (Otte and Pleim, 2010) (hereinafter, M3DRY). We implemented M3DRY in WRF-Chem to examine the O_3 simulation sensitivity for the two different dry deposition schemes using identical input data. We found that both schemes use fairly similar parameterization for the aerodynamic and quasi-laminar resistances, but their surface resistance parameterization differed considerably, as discussed below.

2.3 Surface resistance parameterization

The surface resistance represents the surface uptake of chemical species and depends on the surface chemical and physical characteristics. As the surface resistance decreases, surface uptake of chemical species increases. The surface resistance can be further classified through four specific resistances: the stomata · mesophyll resistance (R_{sm}), cuticle resistance (R_{cut}), in-canopy resistance (R_{inc}), and ground resistance (R_{gnd}). The first three are related to physical and chemical characteristics of vegetation, and the last resistance is related to ground conditions. The four resistances combine in parallel to yield the surface resistance, as follows:

$$\frac{1}{R_c} = \frac{1}{R_{sm}} + \frac{1}{R_{cut}} + \frac{1}{R_{inc}} + \frac{1}{R_{gnd}}. \quad (3)$$

Therefore, the resistance with the smallest value largely determines the surface resistance. Typically, the stomata · mesophyll and ground resistances are the smallest. The stomata · mesophyll resistance is related to vegetation photosynthetic activity, and

ACPD
14, 919–951, 2014

thus, it is a function of solar radiation. During the day, the stomata·mesophyll resistance substantially decreases, and it has the smallest value among the four, although its diurnal variation differs depending on the vegetation type. However, at night, its value becomes higher than the ground resistance, which plays a key role in determining surface resistance without solar radiation. In models, the four resistances shown in Eq. (3) are calculated using complex parameterizations; a detailed discussion on this subject is beyond the scope of our work.

We conducted two WRF-Chem simulations for March–May 2004 in East Asia using the two dry deposition schemes, Wesely and M3DRY. Identical boundary and initial conditions were used for the model, including species emissions, except for the dry deposition scheme. Therefore, the differences in the results are entirely due to the dry deposition calculation differences from each method. The model simulation for March–April was used for spin-up, and we primarily focused our analysis on the results for May here and elsewhere.

2.4 Observations

We used observations from the Bio-hydro-atmosphere interactions of Energy, Aerosols, Carbon, H_2O, Organics, and Nitrogen-Rocky Mountain Organic Carbon Study (BEACHON-ROCS) campaign conducted at the Manitou forest observatory in the United States by NCAR 7–31 August 2010. Details on this campaign are at the following website (https://wiki.ucar.edu/display/mfo/Manitou+Forest+Observatory). We used the gradient method from Tsai et al. (2010) to generate the measured O_3 dry deposition velocity, as shown below. We first estimated ozone flux as a product of the friction velocity and the ozone eddy concentration. The ozone eddy concentration (c^*) can be calculated using Eq. (4) as follows:

$$c^* = k\Delta c \left[\ln\left(\frac{z_0 - d_0}{z_1 - d_0}\right) - \Psi_h\left(\frac{z_2 - d_0}{L}\right) + \Psi_h\left(\frac{z_1 - d_0}{L}\right) \right], \quad (4)$$

ACPD
14, 919–951, 2014

where k is the von Karman constant, and Δc represents the ozone concentration difference between two different observation levels, z_1 (12 m) and z_2 (25 m). d_0 is the zero-plane displacement height, L is the Monin–Obukhov length, and integrated stability function (Ψ_h) is from Businger et al. (1971). After calculating the ozone flux, the dry deposition velocity was calculated by dividing the ozone flux by the ozone concentration at level 2 (z_2). Herein, we only considered the measured dry deposition velocities in the range 0 to 2.0 cm s^{-1}, which is a typical O_3 dry deposition velocity range in the literature (Padro, 1996). The variation in zero-plane displacement height (d_0) can generate a large uncertainty that is proportional to the vegetation height (15 m at the Manitou forest observatory). This variation can be accounted for by applying linear coefficients that range from 0.55 to 0.78 for the vegetation height (Garratt, 1994; Lovett and Reiners, 1986; Perrier, 1982). We computed a range of measured dry deposition velocities with minimum and maximum linear coefficients.

We also used O_3 dry deposition velocities directly measured using the eddy covariance method at a Niwot Ridge AmeriFlux site in the Roosevelt National Forest in the Rocky Mountains of Colorado (Turnipseed et al., 2009). Details for this site are at the following website: http://ameriflux.ornl.gov/fullsiteinfo.php?sid=34.

To evaluate the O_3 simulation, we used surface air O_3 observations at sites from the National Institute of Environmental Research (NIER) in Korea and from the Acid Deposition Monitoring Network in East Asia (EANET, http://www.eanet.asia). The Korean sites are primarily located in polluted urban regions, including Seoul, the capital of South Korea, and Pusan, the second largest city in South Korea, whereas the EANET sites are primarily in islands, rural regions and mountains and were selected to avoid a direct influence from local pollution (Fig. 3). Despite the observation sites in China, O_3 observations are not available to the public, which limits our discussion on observed O_3 spatial patterns. Therefore, we primarily focused on the downwind regions of the continental pollution outflow, which was successfully used in a previous analysis during the TRACE-P campaign to chemically characterize East Asia (Jacob et al., 2003).

ACPD
14, 919–951, 2014

The observations were averaged over the model grid boxes for comparison with the model.

3 O_3 dry deposition velocity spatial and diurnal patterns in East Asia

Figure 1 compares the calculated monthly mean O_3 dry deposition velocities using the Wesely and M3DRY schemes for East Asia. The values are typically high on the continent relative to the ocean, which reflects the decrease in surface resistance due to vegetation. However, as shown in Fig. 1c, we found substantial differences in calculated dry deposition velocities between the two methods. The Wesely method typically yields in greater values compared with M3DRY due to the lower surface resistances in the Wesely method. We also used the two methods to compare the calculated stomata·mesophyll and ground resistances, which are two of the most important factors that affect surface resistance (not shown). We found that the Wesely method typically yields lower values for both the stomata-mesophyll and ground resistance compared with M3DRY. As a result, the Wesely method dry deposition velocity is greater than for the M3DRY method both during the day and at night. The dry deposition velocity domain mean difference between the two methods is 0.14 $cm\,s^{-1}$, which is 1.4 greater than the M3DRY method domain mean dry deposition velocity (0.10 $cm\,s^{-1}$), implying a more rapid O_3 dry deposition loss with the Wesely method.

We evaluated the dry deposition velocities calculated using the two schemes by comparing such values with the observations and primarily focusing on the diurnal variability. The observation values were acquired from the BEACHON_ROCS and Niwot Ridge AmeriFlux sites. Figure 2 compares the hourly measured and simulated O_3 dry deposition velocities using the Wesely and M3DRY methods. The measured values at the BEACHON_ROCS site were greatest in the early morning and decreased toward the afternoon, which reflects the friction velocity diurnal variation that depends on solar radiation. The measured values from the AmeriFlux site also show similar diurnal variation; the greatest values were from the afternoon. The simulation results from

ACPD
14, 919–951, 2014

the Wesely method were consistent with the observations and reproduced the diurnal variation, whereas the M3DRY method results were significantly lower than the observations. As discussed above, during the day, the stomata resistance was the most dominant factor for determining the dry deposition velocity and was better resolved in the Wesely method than the M3DRY method.

Our comparison in Fig. 2 shows that the Wesely method is better than M3DRY. Although this result is based on a comparison from the United States, we believe that this evaluation can be applied to East Asia. The Manitou forest observatory is a ponderosa pine plantation in the middle of shrub land (Kim et al., 2010), which is prevalent in East Asia, especially in the middle of China, as shown in Fig. 5a. We acknowledge that our evaluation is limited to a single type of vegetation, which does not represent East Asia in its entirety. In-situ O_3 dry deposition velocity measurements are critical and necessary for enhancing our understanding of O_3 loss and modeling capability for East Asia.

4 O_3 concentration spatial and diurnal patterns in East Asia

Figure 3 shows the observed and simulated monthly mean O_3 concentrations in the surface air over East Asia in May 2004 using the Wesely and M3DRY schemes. The observed values show a spatial gradient, wherein values at polluted urban sites in Korea are lower than at clean rural sites in Japan. O_3 loss through high NO emissions from automobiles in large megacities explains this observed spatial pattern with low values in Korea.

The simulated O_3 concentrations also show a clear spatial gradient, which is high over the downwind ocean and relatively low over the continent, where its precursor emissions are generated. Generally, the model reflects the observed spatial pattern with low values in Korea and high values in Japan.

However, the most striking feature is that the simulated values from the Wesely scheme are lower than from the M3DRY scheme. The O_3 difference between the two

ACPD
14, 919–951, 2014

methods is up to 10 ppbv for the monthly mean and 4.7 ppbv averaged over the entire domain (Fig. 3c). The largest differences are in the Yellow Sea and northwestern Pacific, wherein the O_3 loss through dry deposition is weaker relative to the continent, as shown in Sect. 3.

The largest dry deposition velocity differences that we calculated were on the continents; however, the O_3 concentrations differences were greatest for the downwind ocean (Fig. 3). These data indicate that O_3 efficiently exports from the polluted continent to the downwind oceans, where O_3 accumulates due to relatively inefficient dry depositional loss. In addition, the O_3 differences over the ocean may partially be attributed to excessively high surface water resistance (low deposition loss) in the M3DRY scheme relative to the Wesely scheme, which is not clearly shown in Fig. 1. This issue is discussed in Sect. 5.

Figure 4 shows the hourly mean observed and simulated O_3 concentrations at the NIER sites in Korea and EANET sites in Japan. The values were computed by averaging the hourly data from individual sites. We also sampled the corresponding model-grid values at individual sites for this comparison. The diurnal O_3 concentration variation differs between the two networks such that the observed O_3 concentrations in Korea show a strong diurnal variation, a peak in the afternoon and a minimum at night, which reflects direct influence from local pollution. However, such diurnal variation is less pronounced at the EANET sites.

The model reflects the observed temporal variation well. However, we also found considerable discrepancies between the model and observations. For example, at the NIER sites in Korea, the M3DRY method overestimated the observations by 4.4–17.1 ppbv. This high bias was lower when we used the Wesely method; although, the model did not reflect the lowest O_3 concentrations in the early morning. The lowest O_3 levels observed might be due to the chemical loss through NO during the early morning rush hour. We further examine this issue in Sect. 5.

The O_3 concentration values from the model are generally lower than the observed values at the EANET sites. This bias toward lower values is also exhibited by the model

ACPD
14, 919–951, 2014

using both dry deposition schemes; although, the M3DRY scheme is more consistent with the observations. In general, the model and observation discrepancies are due to the model's inability to simulate steep sub-grid land-to-sea gradients at a mixing depth (Gao and Wesely, 1994) that is shallower over the ocean compared with the continent. Our model with 45 km × 45 km spatial resolution may not adequately reflect the shallow mixing depth at the EANET sites, which are near the sea.

Although the model reflects certain observed features, using the comparisons in Figs. 3 and 4, it is difficult to determine the scheme with the best performance at reproducing the observed O_3 concentration spatial and temporal variations in East Asia. However, as discussed in Sect. 3, the model using the Wesely scheme reproduced the observed dry deposition velocities better than M3DRY. Therefore, we used the Wesely scheme results for our subsequent analysis below, where we examined the model's sensitivity for other input parameters.

5 Surface-type uncertainty effects on the simulated O_3 concentrations

The dry deposition velocity spatial distribution closely resembles the land-use data, which indicates that the model is highly sensitive to land-use data. The land-use information from the United States Geological Survey (USGS) was used as the default for WRF-Chem. Here, we compare the USGS data with the MODIS land-use data (Friedl et al., 2002), which is widely used in meteorological research; we also explore the model sensitivity to the different surface-type specifications. First, the two datasets use a different coding system for denoting each surface type. For example, the USGS uses eight for the shrub land, whereas the MODIS uses six. The two data sets were difficult to compare due to the different coding systems. Therefore, as shown in Table 4, we developed a mapping table for the surface type using the two datasets, and this mapping information was used to implement the MODIS land-use data in the WRF-Chem simulations below.

ACPD
14, 919–951, 2014

Figure 5 shows the USGS and MODIS land-use data. The color-coding system used for the individual surface types is consistent with the USGS coding system (Tables 3 and 4). In general, vegetation types identified by the two datasets are consistent for East Asia, but the datasets yield certain differences, especially for south China. One notable difference is that USGS classifies the Korean peninsula as a Savanna (code 10 in Table 3), which differs from the MODIS classification (mixed forest, code 5 in Table 4). The different surface-type classifications affect O_3 dry deposition in the model, and we examine the simulated O_3 sensitivity to the surface types below.

Figure 6 shows the dry deposition velocity and O_3 concentration differences in the model using two different surface-type datasets: MODIS and USGS. Here, we use the Wesely dry deposition scheme, for which the simulated dry deposition velocities were consistent with the observations and which was more sensitive to surface types than M3DRY. Therefore, the dry deposition velocity differences reflect the different surface-type classifications between the two datasets. Generally, we calculated lower dry deposition velocities for East Asia using MODIS compared with USGS. Southern China yields the greatest decrease, for which the surface type was changed from cropland/pasture, cropland/grassland mosaic, shrubland, and savanna to mixed forest (Fig. 5). The surface-type differences increased the surface resistances and, thus, decreased the dry deposition velocity. On the other hand, the calculations for Manchuria and Republic of the Union of Myanmar showed higher dry deposition velocities because the surface type was changed from mixed forest to cropland/pasture or evergreen broadleaf.

The dry deposition velocity changes significantly increased the O_3 concentration up to a 1.2 ppbv monthly mean in southern China and the downwind regions, including Korea, Japan and the north Pacific. The average O_3 concentration over the domain using the MODIS land-use data was slightly higher (by 1.3 %) compared with the USGS data. However, in the urban and industrialized regions, the O_3 increase from MODIS was greater (by 5.1 ppbv; 12.7 %) compared with the USGS data, which indicates that the surface-type classification is important for the O_3 simulations.

ACPD
14, 919–951, 2014

Figure 7 compares the model results from the two different surface datasets with the observations. We found that the simulated O_3 concentrations were highly sensitive at NIER sites in Korea, where the surface type changes from Savanna to the mixed forest, urban and built-up land generates a 3.9 ppbv monthly mean increase, which is slightly worse for the model results compared with the observations. The model spatial resolution was too coarse to represent surface-type inhomogeneity in Korea at the NIER sites, which are primarily in urban regions. The surface-type sub-grid scale variability may also be a potentially important source for model uncertainty. On the other hand, the model shows minimal changes in O_3 at the EANET sites located near the sea.

We further examine sensitivity for the simulated O_3 at different surface water resistances using the dry deposition schemes. The Wesely scheme used 2000 $s\,m^{-1}$ for the water resistance, which was lower than the M3DRY scheme water resistance ($10^5 \sim 10^6$ $s\,m^{-1}$). We conducted a model simulation using the Wesely scheme by switching the water surface resistance values from the Wesley to the M3DRY values. Figure 8 shows the resulting dry deposition velocity and O_3 concentration differences from the model. We found that the dry deposition velocity increased up to 0.043 $cm\,s^{-1}$, which yielded an O_3 decrease as low as 8.7 ppbv in the ocean; this change is 76 % of the previous overall O_3 concentration difference between the two schemes for the ocean. Although the O_3 dry deposition loss is lower in the ocean compared with the continent, this result indicates that the model is highly sensitive to water surface resistance, which has an important implication for estimating long-range O_3 transport from a source to receptor.

Finally, we conducted a nested model simulation using a finer spatial resolution (15 km) and focusing on the Korean peninsula to examine the effect of NO titration on O_3 concentrations in polluted urban cities. Figure 9 compares the simulated O_3 concentrations from the nested model with the observations at the NIER sites in Korea. With the finer spatial resolution, the nested model yielded lower O_3 concentrations due to NO titration because the concentrated NO emissions were better represented

ACPD
14, 919–951, 2014

compared with the coarse model. We found the greatest reduction during the early morning, when the NO emission from rush hour traffic is greatest, as shown in Fig. 9b. However, the model's high bias for the early morning remains, which indicates that the nested model is still too coarse to represent the concentrated plume from traffic.

6 Conclusions

We used the WRF-Chem with two widely used dry deposition schemes (Wesely and M3DRY) to evaluate such schemes and examine the sensitivity of the simulated surface air O_3 concentrations to dry deposition calculations for East Asia. We found significant differences in O_3 concentrations up to 10 ppbv for the monthly mean, primarily due to the dry deposition velocity differences between the two schemes. The Wesely scheme generates 1.4 times greater dry deposition velocity values compared with M3DRY under identical meteorological conditions due to discrepancies in the surface resistance parameterization. Among the surface resistances, the mesophyll and stomata resistances were the most importance factors during the day, whereas the ground resistance was an important factor for the continent at night. In addition, the surface resistance of the sea can yield considerable O_3 concentration differences over the ocean.

We compared the simulated dry deposition velocities with the observed dry deposition velocity from the BEACHON-ROCS campaign. The Wesely scheme reproduced the observed dry deposition velocity diurnal variation better than the M3DRY scheme. The Wesely scheme also reproduced the observed diurnal O_3 concentration variation at polluted urban sites in Korea but failed to reflect the observations at relatively clean sites in Japan, which indicates that other factors are important for O_3 simulations in East Asia, such as emission, chemistry, and meteorology.

We conducted several sensitivity simulations for the land-use data, water surface resistance and model spatial resolution to examine uncertainty in O_3 concentration simulations for East Asia. The model results showed considerable changes in the simulated O_3 concentrations, which suggests that the model is highly sensitive to such

ACPD
14, 919–951, 2014

input data and the model resolution. Observations are necessary to constrain the dry deposition parameterization and input data and improve East Asia air quality models.

The roles of vegetation have primarily been discussed for reactive BVOC emissions and tropospheric photochemistry that enhances O_3 and SOA production in East Asia air quality research (e.g., Kim et al., 2013; Bao et al., 2011; Ran et al., 2011; Tie et al., 2013). Therefore, the comprehensive evaluation of dry deposition model schemes herein clearly indicates that deposition is also a critical physical process, which must be precisely constrained in regional and global air quality assessments because O_3 has tremendous implications for public health (Levy et al., 2001) and climate change (IPCC, 2007). In addition, a number of experimental studies have clearly suggested that a substantial level of unknown/unobserved reactive BVOCs may enhance non-stomatal O_3 dry deposition rates (Kurpius and Goldstein, 2003; Hogg et al., 2007); chemical processes should also be empirically evaluated and incorporated in regional models.

Acknowledgements. This study was supported by the Korea Meteorological Administration Research and Development Program under the Grant CATER 2012–6121 and the National Research Foundation of Korea (NRF) grant funded by the Korean government (MSIP) (2009-83527). The National Center for Atmospheric Research is operated by the University Corporation for Atmospheric Research under sponsorship from the National Science Foundation. Any opinions, findings and conclusions or recommendations expressed in this publication are those of the authors and do not necessarily reflect the views of the National Science Foundation.

References

Appel, K. W., Gilliland, A. B., Sarwar, G., and Gilliam, R. C.: Evaluation of the Community Multiscale Air Quality (CMAQ) model version 4.5: sensitivities impacting model performance: Part I – ozone, Atmos. Environ., 41, 9603–9615, 2007.

Bao, H., Shrestha, K. L., Kondo, A., Kaga, A., and Inoue, Y.: Modeling the influence of biogenic volatile organic compound emissions on ozone concentration during summer season in the Kinki region of Japan, Atmos. Environ., 44, 421–431, 2010.

ACPD
14, 919–951, 2014

Businger, J. A., Wyngaard, J. C., Izumi, I., and Bradley, E. F.: Flux-profile relationships in the atmospheric surface layer, J. Atmos. Sci., 28, 181–189, 1971.
Byun, D. W. and Ching, J. K. S.: Science algorithms of the EPA Models3 Community Multiscale Air Quality (CMAQ) Modeling System, EPA600/R99/030, USEPA, 1999.
Chapman, E. G., Gustafson Jr., W. I., Easter, R. C., Barnard, J. C., Ghan, S. J., Pekour, M. S., and Fast, J. D.: Coupling aerosol-cloud-radiative processes in the WRF-Chem model: investigating the radiative impact of elevated point sources, Atmos. Chem. Phys., 9, 945–964, doi:10.5194/acp-9-945-2009, 2009.
Charusombat, U., Niyogi, D., Kumar, A., Wang, X., Chen, F., Guenther, A., Turnipseed, A., and Alapaty, K.: Evaluating a new deposition velocity module in the Noah Land – Surface Model, Bound.-Lay. Meteorol., 137, 271–290, 2010.
Chen, F. and Dudhia, J.: Coupling an advanced land surface – hydrology model with the Penn State – NCAR MM5 Modeling System, Part I: model implementation and sensitivity, Mon. Weather Rev., 129, 569–585, 2001.
Erisman, J. W., Vanpul, A., and Wyers, P.: Parametrization of surface-resistance for the quantification of atmospheric deposition of acidifying pollutants and ozone, Atmos. Environ., 28, 2595–2607, 1994.
Friedl, M. A., McIver, D. K., Hodges, J. C. F., Zhang, X. Y., Muchoney, D., Strahler, A. H., Woodcock, C. E., Gopal, S., Schneider, A., Cooper, A., Baccini, A., Gao, F., and Schaaf, C.: Global land cover mapping from MODIS: algorithms and early results, Remote Sens. Environ., 83, 287–302, 2002.
Gao, W. and Wesely, M. L.: Numerical modeling of the turbulent fluxes of chemically reactive trace gases in the atmospheric boundary-layer, J. Appl. Meteorol., 33, 835–847, 1994.
Garratt, J. R.: The Atmospheric Boundary Layer, Cambridge University Press, 86, 1994.
Gerosa, G., Derghi, F., and Cieslik, S.: Comparison of different algorithms for stomatal ozone flux determination from micrometeorological measurements, Water Air Soil Poll., 179, 309–321, 2007.
Grell, G. A., Peckham, S. E., Schmitz, R., McKeen, S. A., Frost, G., Skamarock, W. C., and Eder, B.: Fully coupled "online" chemistry within the WRF model, Atmos. Environ., 39, 6957–6975, 2005.
Hogg, A., Uddling, J., Ellsworth, D., Carroll, M. A., Pressley, S., Lamb, B., and Vogel, C.: Stomatal and non-stomatal fluxes of ozone to a northern mixed hardwood forest, Tellus B, 59, 514–525, doi:10.1111/J.1600-0889.2007.00269.X, 2007.

ACPD
14, 919–951, 2014

Hong, S.-Y., Noh, Y., and Dudhia, J.: A new vertical diffusion package with an explicit treatment of entrainment processes, Mon. Weather Rev., 134, 2318–2341, 2006.
IPCC: Climate Change 2007: The Scientific Basis, Cambridge Univ. Press, New York, 2007.
Jacob, D. J., Crawford, J. H., Kleb, M. M., Connors, V. S., Bendura, R. J., Raper, J. L., Sachse, G. W., Gille, J. C., Emmons, L., and Heald, C. L.: Transport and Chemical Evolution over the Pacific (TRACE-P) aircraft mission: design, execution, and first results, J. Geophys. Res.-Atmos., 108, 9000, 2003.
Kim, S., Karl, T., Guenther, A., Tyndall, G., Orlando, J., Harley, P., Rasmussen, R., and Apel, E.: Emissions and ambient distributions of Biogenic Volatile Organic Compounds (BVOC) in a ponderosa pine ecosystem: interpretation of PTR-MS mass spectra, Atmos. Chem. Phys., 10, 1759–1771, doi:10.5194/acp-10-1759-2010, 2010.
Kim, S., Lee, M., Kim, S., Choi, S., Seok, S., and Kim, S.: Photochemical characteristics of high and low ozone episodes observed in the Taehwa Forest observatory (TFO) in June 2011 near Seoul South Korea, Asia-Pac. J. Atmos. Sci., 49, 325–331, 2013.
Kurpius, M. R. and Goldstein, A. H.: Gas-phase chemistry dominates O_3 loss to a forest, implying a source of aerosols and hydroxyl radicals to the atmosphere, Geophys. Res. Lett., 30, 1371 doi:10.1029/2002gl016785, 2003.
Lelieveld, J. and Dentener, F. J.: What controls tropospheric ozone?, J. Geophys. Res., 105, 3531–3551, 2000.
Levy, J. I., Carrothers, T. J., Tuomisto, J. T., Hammitt, J. K., and Evans, J. S.: Assessing the public health benefits of reduced ozone concentrations, Environ. Health Persp., 109, 1215–1226, 2001.
Lovett, G. M. and Reiners, W. A.: Canopy structure and cloud water deposition in subalpine coniferous forests, Tellus B, 38, 319–327, 1986.
Matsuda, K., Watanabe, I., and Wingpud, V.: Ozone dry deposition above a tropical forest in the dry season in northern Thailand, Atmos. Environ., 39, 2571–2577, 2005.
Matsuda, K., Watanabe, I., Wingpud, V., Theramongkol, P., and Ohizumi, T.: Deposition velocity of O_3 and SO_2 in the dry and wet season above a tropical forest in northern Thailand, Atmos. Environ., 40, 7557–7564, 2006.
National Centers for Environmental Prediction, N.W.S.N.U.S.D.o.C.: NCEP FNL Operational Model Global Tropospheric Analyses, continuing from July 1999, Research Data Archive at the National Center for Atmospheric Research, Computational and Information Systems Laboratory, Boulder, CO, 2000.

ACPD
14, 919–951, 2014

Ohara, T., Akimoto, H., Kurokawa, J., Horii, N., Yamaji, K., Yan, X., and Hayasaka, T.: An Asian emission inventory of anthropogenic emission sources for the period 1980–2020, Atmos. Chem. Phys., 7, 4419–4444, doi:10.5194/acp-7-4419-2007, 2007.

Otte, T. L. and Pleim, J. E.: The Meteorology-Chemistry Interface Processor (MCIP) for the CMAQ modeling system: updates through MCIPv3.4.1, Geosci. Model Dev., 3, 243–256, doi:10.5194/gmd-3-243-2010, 2010.

Padro, J.: Summary of ozone dry deposition velocity measurements and model estimates over vineyard, cotton, grass and deciduous forest in summer, Atmos. Environ., 30, 2363–2369, 1996.

Perrier, A.: Land surface processes: vegetation, in: Land Surface Processes in Atmospheric General Circulation Models, Cambridge University Press, 395–448, 1982.

Pleim, J. E., Xiu, A., Finkelstein, P. L., and Otte, T. L.: A coupled land–surface and dry deposition model and comparison to field measurements of surface heat, moisture, and ozone fluxes, Water Air Soil Poll., 1, 243–252, 2001.

Ran, L., Zhao, C. S., Xu, W. Y., Lu, X. Q., Han, M., Lin, W. L., Yan, P., Xu, X. B., Deng, Z. Z., Ma, N., Liu, P. F., Yu, J., Liang, W. D., and Chen, L. L.: VOC reactivity and its effect on ozone production during the HaChi summer campaign, Atmos. Chem. Phys., 11, 4657–4667, doi:10.5194/acp-11-4657-2011, 2011.

Rannik, Ü., Altimir, N., Mammarella, I., Bäck, J., Rinne, J., Ruuskanen, T. M., Hari, P., Vesala, T., and Kulmala, M.: Ozone deposition into a boreal forest over a decade of observations: evaluating deposition partitioning and driving variables, Atmos. Chem. Phys., 12, 12165–12182, doi:10.5194/acp-12-12165-2012, 2012.

Tie, X., Geng, F., Guenther, A., Cao, J., Greenberg, J., Zhang, R., Apel, E., Li, G., Weinheimer, A., Chen, J., and Cai, C.: Megacity impacts on regional ozone formation: observations and WRF-Chem modeling for the MIRAGE-Shanghai field campaign, Atmos. Chem. Phys., 13, 5655–5669, doi:10.5194/acp-13-5655-2013, 2013.

Tsai, J. L., Chen, C. L., Tsuang, B. J., Kuo, P. H., Tseng, K. H., Hsu, T. F., Sheu, B. H., Liu, C. P., and Hsueh, M. T.: Observation of SO_2 dry deposition velocity at a high elevation flux tower over an evergreen broadleaf forest in Central Taiwan, Atmos. Environ., 44, 1011–1019, 2010.

Turnipseed, A. A., Burns, S. P., Moore, D. J. P., Hu, J., Guenther, A. B., and Monson, R. K.: Controls over ozone deposition to a high elevation subalpine forest, Agr. Forest Meteorol., 149, 1447–1459, 2009.

ACPD
14, 919–951, 2014

Wesely, M. L.: Parameterization of surface resistances to gaseous dry deposition in regional-scale numerical models, Atmos. Environ., 23, 1293–1304, 1989.
Woo, J.-H., Choi, K.-C., Kim, H. K., Baek, B. H., Jang, M., Eum, J.-H., Song, C. H., Ma, Y.-I., Sunwoo, Y., Chang, L.-S., and Yoo, S. H.: Development of an anthropogenic emissions processing system for Asia using SMOKE, Atmos. Environ., 58, 5–13, 2011.
Wu, S., Mickley, L. J., Jacob, D. J., Logan, J. A., Yantosca, R. M., and Rind, D.: Why are there large differences between models in global budgets of tropospheric ozone?, J. Geophys. Res., 112, D05302, doi:10.1029/2006JD007801, 2007.
Wu, Z., Wang, X., Chen, F., Turnipseed, A. A., Guenther, A. B., Niyogi, D., Charusombat, U., Xia, B., William Munger, J., and Alapaty, K.: Evaluating the calculated dry deposition velocities of reactive nitrogen oxides and ozone from two community models over a temperate deciduous forest, Atmos. Environ., 45, 2663–2674, 2011.

ACPD
14, 919–951, 2014

Table 1. Physics options used in the WRF-Chem simulations.

Feature	Selected configuration
Domain	East Asia on 45 km grid with 14 layers
Domain top	50 hPa
Emission	SMOKE-ASA (Only anthropogenic)
Longwave radiation	RRTM
Shortwave radiation	Goddard
Microphysics	Lin (Purdue)
Cumulus parameterization	Grell–Devenyi
Vertical diffusion	Eddy
Chemical mechanism	CBz
Surface layer physics	Monin–Obukhov
Land surface model	Noah
Planetary boundary layer	YSU
Photolysis	Fast-J

ACPD
14, 919–951, 2014

Table 2. Species mapping using the CB05 and CBz chemical schemes.

CBz (WRF-Chem)	CB05	CBz	CB05
E_ALD	ALD2+ALDX	E_TOL	TOL
E_CO	CO	E_XYL	XYL
E_OL2	ETH	E_ETH	ETHA
E_HCHO	FORM	E_C2H5OH	ETOH
E_ISOP	ISOP	E_OLI	IOLE
E_NH3	NH3	E_CH3OH	MEOH
E_NO	NO		NASN
E_NO2	NO2		TERP
E_OLE	OLE	E_KET	
E_PAR	PAR	E_ORA2	
E_SO2	SO2	E_CLS	

* NASN, TERP, E_KET, E_ORA2, and E_CLS have no corresponding species.

ACPD
14, 919–951, 2014

Table 3. USGS 24 land-use data categories.

Land Use Category	Land Use Description
1	Urban and Built-up Land
2	Dryland Cropland and Pasture
3	Irrigated Cropland and Pasture
4	Mixed Dryland/Irrigated Cropland and Pasture
5	Cropland/Grassland Mosaic
6	Cropland/Woodland Mosaic
7	Grassland
8	Shrubland
9	Mixed Shrubland/Grassland
10	Savanna
11	Deciduous Broadleaf Forest
12	Deciduous Needleleaf Forest
13	Evergreen Broadleaf
14	Evergreen Needleleaf
15	Mixed Forest
16	Water Bodies
17	Herbaceous Wetland
18	Wooden Wetland
19	Barren or Sparsely Vegetated
20	Herbaceous Tundra
21	Wooded Tundra
22	Mixed Tundra
23	Bare Ground Tundra
24	Snow or Ice

ACPD
14, 919–951, 2014

Table 4. Land-use mapping using the 20-category IGBP-Modified MODIS and 24-category USGS schemes.

MODIS	USGS	MODIS	USGS
Evergreen Needeleleaf Forest	Evergreen Needleleaf	1	14
Evergreen Broadleaf Forest	Evergreen Broadleaf	2	13
Deciduous Needleleaf Forest	Deciduous Needleleaf Forest	3	12
Deciduous broadleaf Forest	Deciduous Broadleaf Forest	4	11
Mixed Forest	Mixed Forest	5	15
Closed Shrubland	Shrubland	6	8
Open Shrubland	Mixed Shrubland/Grassland	7	9
Woody Savanna	Savanna	8	10
Savanna	Savanna	9	10
Grassland	Grassland	10	7
Permanents Wetland	Herbaceous Wetland	11	17
Cropland	Irrigated Cropland and Pasture	12	3
Urban and Built-up	Urban and Built-up Land	13	1
Cropland/Natural Mosaic	Cropland/Grassland Mosaic	14	5
Snow and Ice	Snow or Ice	15	24
Barren or Sparsely Vegetated	Barren or Sparsely Vegetated	16	19
Water	Water Bodies	17	16
Wooded Tundra	Wooded Tundra	18	21
Mixed Tundra	Mixed Tundra	19	22
Barren Tundra	Bare Ground Tundra	20	23

ACPD
14, 919–951, 2014

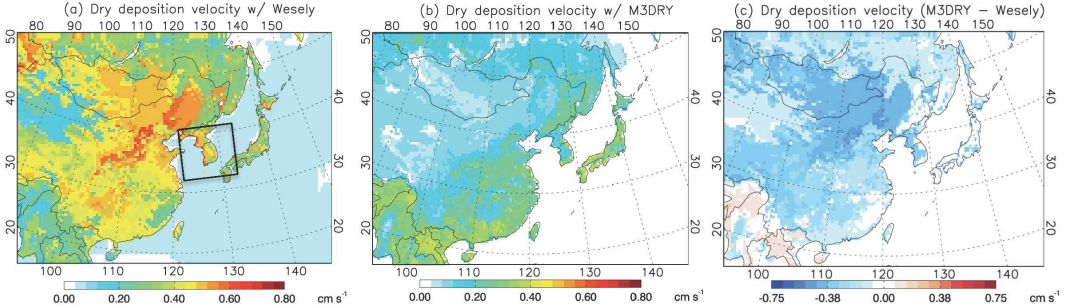

Fig. 1. The O_3 monthly mean dry deposition velocities in East Asia for May 2004 from WRF-Chem using the Wesely (left) and M3DRY schemes (middle). The different values from the two simulations are shown in the right panel.

ACPD
14, 919–951, 2014

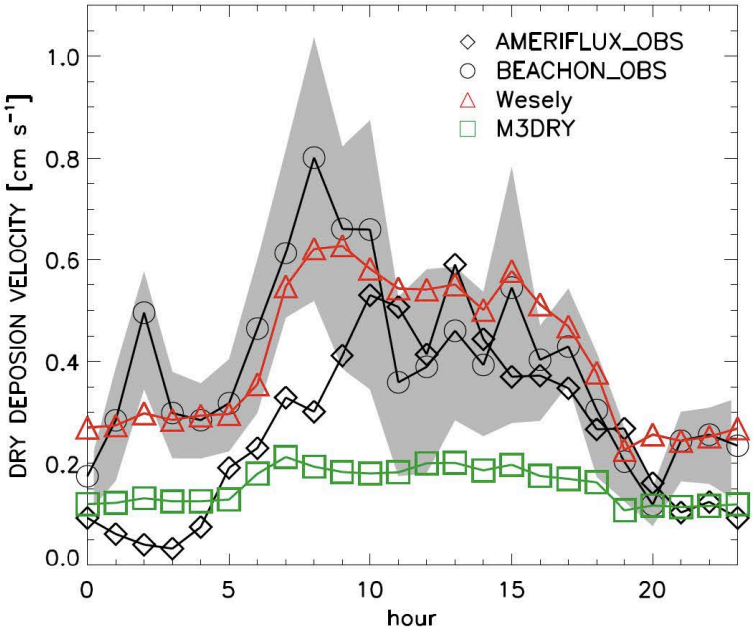

Fig. 2. A comparison of the simulated and observed hourly mean O_3 dry deposition velocities from the Niwot Ridge AmeriFlux site in the Roosevelt National Forest in the Rocky Mountains of Colorado (diamonds) and from the BEACHON-ROCS campaign conducted at the Manitou forest observatory (circles) in the United States. The triangles and squares show the simulated values using the Wesely and M3DRY schemes, respectively. The shaded area indicates the observed dry deposition velocity range for the various zero-plane displacement heights (d_0) in Eq. (4) from the BEACHON-ROCS campaign.

ACPD
14, 919–951, 2014

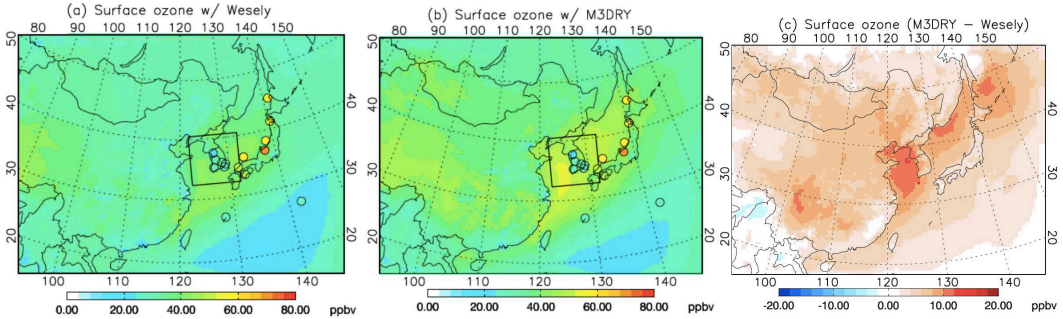

Fig. 3. Monthly mean O_3 concentrations in East Asia surface air for May 2004. The left and middle panels show results from the WRF-Chem model using identical emission and meteorological input data but different dry deposition schemes, **(a)** Wesely and **(b)** M3DRY. Observations from the NIER and EANET sites are denoted using colored closed circles. The O_3 concentration differences between the two simulations are shown in the right panel **(c)**.

ACPD
14, 919–951, 2014

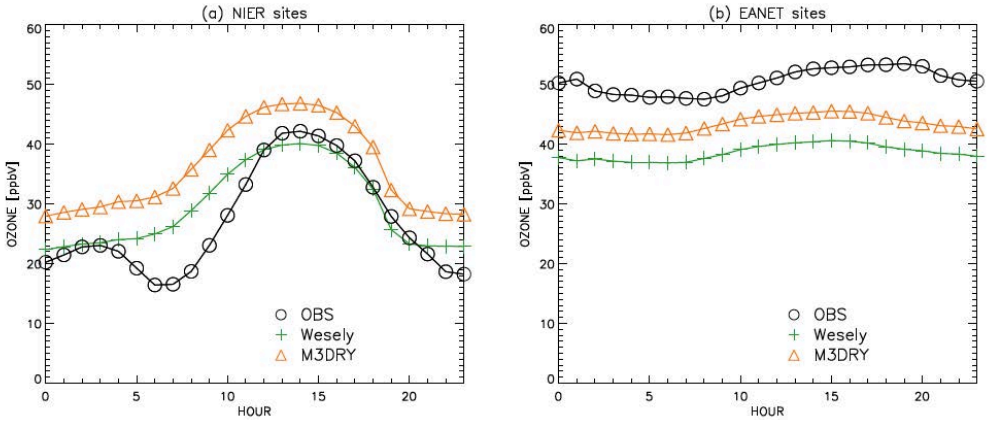

Fig. 4. Hourly mean O_3 concentrations averaged over **(a)** the NIER sites (left) and **(b)** EANET sites (right) for May 2004. The simulated values were sampled from the model grids, which correspond to the site locations. The observations are denoted with open circles, and the simulated values from Wesely and M3DRY are shown using pluses and triangles, respectively.

ACPD
14, 919–951, 2014

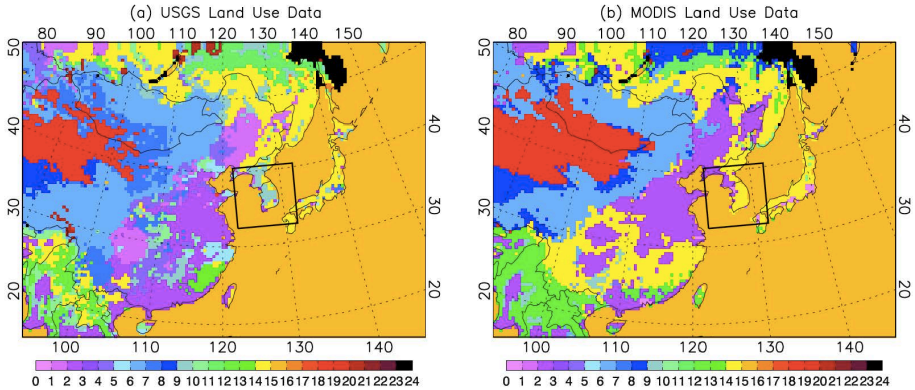

Fig. 5. Land-use data from the USGS (left) and MODIS datasets (right). The color-coding scheme used to denote the different surface types are consistent for the datasets and follow the USGS dataset coloring (Table 3). We used the mapping information (Table 4) to illustrate the MODIS data.

ACPD
14, 919–951, 2014

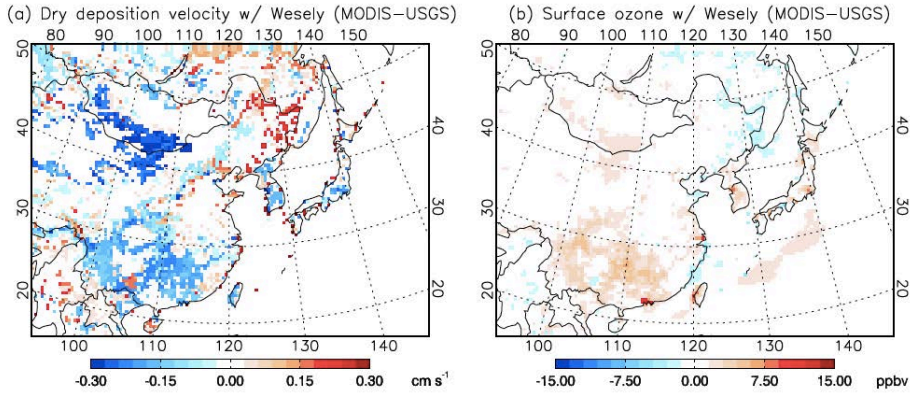

Fig. 6. Differences in dry deposition velocity (left) and monthly mean O_3 concentration in the surface air (right) between the MODIS and USGS land-use data using the Wesely scheme for May 2004.

ACPD
14, 919–951, 2014

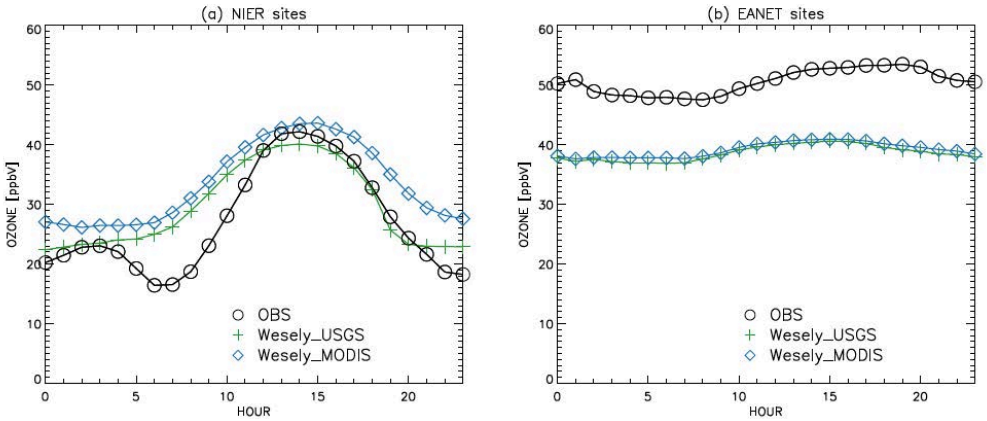

Fig. 7. The data are the same as in Fig. 2, except that the simulated O_3 concentrations were generated using the USGS (pluses) and MODIS land-use data (diamonds) with the Wesely scheme.

ACPD
14, 919–951, 2014

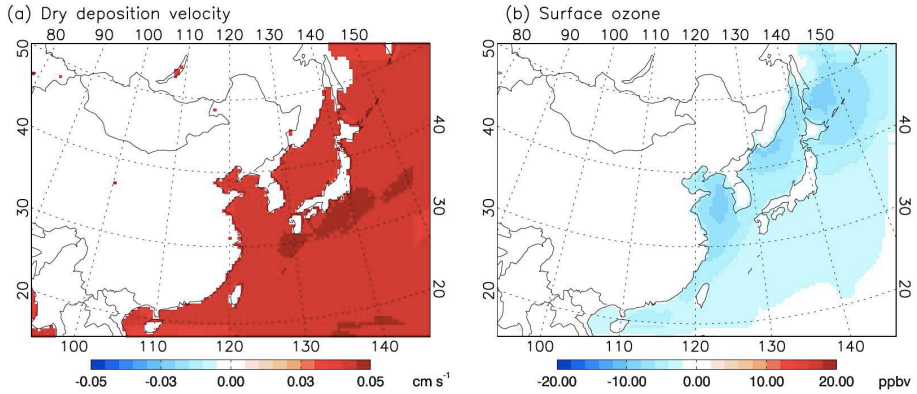

Fig. 8. Differences in dry deposition velocities (left) and monthly mean concentrations in surface air O_3 (right) from the default and sensitivity simulations. The sensitivity simulation was conducted using the Wesely scheme and replacing the ocean surface resistance with the values from the M3DRY scheme.

ACPD
14, 919–951, 2014

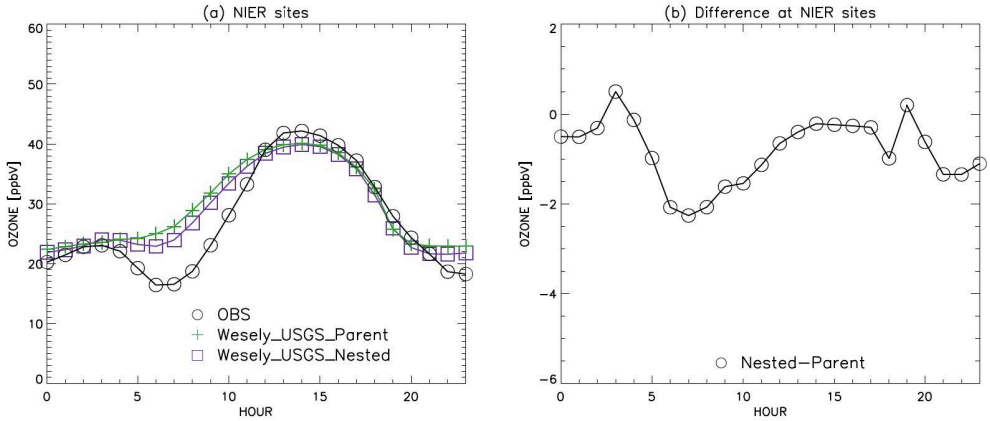

Fig. 9. Hourly mean O_3 concentrations averaged over the NIER sites (left) for May 2004. The pluses and squares indicate results from the default (45 km × 45 km) and nested models (15 km × 15 km), respectively. The observations are denoted with the open circles. The differences between the two models are shown in the right panel.

ACPD
14, 919–951, 2014